The sedimentological signature of impact spherules and its relation to ejecta transport mechanisms during the Chicxulub asteroid impact (Cretaceous/Paleogene boundary)

Hermann D. Bermúdez[1-3*], Liliana Bolívar[2], José A. Arz[4], Ignacio Arenillas[4], Vicente Gilabert[4-5], Robert DePalma[6-7], George Phillips[8], Daniela Bermúdez[9], Maurizia De Palma[1], Clemencia Gómez[3], Ying Cui[1]

[1]Department of Earth and Environmental Studies, Montclair State University, Montclair, NJ 07043, USA.

[2]Grupo de Investigación Paleoexplorer, 1400-37 Trexlertown Rd. PA 18062, USA.

[3]Departamento de Geociencias, Universidad Nacional de Colombia, Bogotá 11001, Colombia.

[4]Departamento de Ciencias de la Tierra-IUCA, Universidad de Zaragoza, E-50009 Zaragoza, Spain.

[5]Departament de Dinàmica de la Terra i de l'Oceà, Universitat de Barcelona, E-08028 Barcelona, Spain.

[6]Department of Earth and Environmental Sciences, University of Manchester, Manchester, M13 9PL, UK.

[7]Department of Geosciences, Florida Atlantic University, Boca Raton, FL 33431, USA.

[8]Mississippi Museum of Natural Science, Conservation & Biodiversity Section, Jackson, MS 39202, USA.

[9]Science and Technology School, Environmental Sciences for Sustainability, Ie University, C. Cardenal Zúñiga, 12, Segovia, Castilla y Leon 40003, Spain.

**Corresponding author: bermudezh@montclair.edu*

ABSTRACT

The Chicxulub impact is the most likely cause of the Cretaceous/Paleogene boundary (KPB) mass extinction and the only impact event in Earth's history with a globally traceable ejecta bed. Although the impact spherules are thought to represent molten or vaporized material, precise genesis and transport mechanisms remain underconstrained. Here, we show that the morphology, size, internal structure, and distribution of the spherules within the KPB deposits are related to origin and transport processes. The study of thousands of spherules from KPB deposits in Colombia, the USA, and Spain has revealed the presence of three fractions related to three different distribution processes, each with a distinctive sedimentological signature. The coarser fraction ("aspergo deposit," from the Latin *aspergo*, meaning splash) comprises rotational and agglutinated/irregular forms (size > 2mm) containing abundant vesicles, unmelted inclusions, and schlieren, implying an origin from molten materials and transport following ballistic trajectories. The intermediate fraction ("pyrocloud deposit" from the Greek *pyr*, meaning fire) represents a mixture of molten and condensed droplets, including spheres, rotational, and agglutinated/irregular forms (size 0.3 - 2 mm), transported by the rapid expansion of a fast-moving, high-temperature turbulent cloud. The globally distributed finer fraction ("fireball layer") is composed exclusively of spheres (size < 0.3 mm) condensed from a vapor plume after the Chicxulub impact. These observations provide valuable insights into ejecta distributions during massive asteroid impacts and enhance our understanding of the Chicxulub impact and its aftermath.

Keywords: Chicxulub, Cretaceous/Paleogene boundary, impact spherules, morphology, ejecta distribution.

1. Introduction

Asteroid impacts are frequent events in the evolution of the Solar System. As a result, impact craters are the most common type of landform in the planetary bodies that compose it (Koeberl, 2002; Simonson and Glass, 2004). While the number of well-documented asteroid impacts on Earth is relatively low, since the Earth's crust is highly dynamic, these events have left a deep imprint on the geological record and the evolution of life (Pierazzo and Artemieva, 2012; Schmieder and Kring, 2020; Osinski et al., 2022;). During the earliest stages of high-velocity impact events, large volumes of vaporized, molten, and crushed material are expelled over large areas, forming an ejecta layer that thins away from the crater (Melosh, 1989; Kring and Durda, 2002; Glass and Simonson, 2012; Osinski et al., 2022). Ejecta deposited less than 2.5 times the impact crater diameter is called proximal ejecta (5 times according to Koeberl, 2002); materials ejected beyond that distance are called distal ejecta (Glass and Simonson, 2012).

Glass produced by melting during impact events is called impact glass or impactite (Koeberl, 1986) and is an important component of the ejecta layers. There is no clarity or agreement on how to describe ejecta composed mainly of impact glass, as there are different terms according to their size, composition, and origin (Rieihart, 1958; Stöffler, 1984; Koeberl, 1986; Glass and Burns, 1988; Koeberl, 1992; Koeberl, 1993; Koeberl, 2002; Elkins-Tanton et al., 2003; Glass and Simonson, 2011; Glass and Simonson, 2012; Glass, 2016; Macris et al., 2018). Nonetheless, we can consider that as it cools down, the ejected material can form large glass bodies centimeters in size or larger, called tektites, and smaller glass bodies, called impact spherules (Glass and Simonson, 2012; Glass, 2016). According to the original description (Suess, 1900), tektites, from the Greek τήκτος - *tektos*, meaning molten, are melt droplets composed entirely of macroscopically homogeneous glass (Rieihart, 1958; Koeberl, 1986; Glass and Burns,

1988; Koeberl, 2002; Glass, 2016). According to the size (Glass and Simonson, 2013), it is possible to subdivide the tektites into micro (<1 mm diameter), mini (1-10 mm diameter), and macrotektites (>10 mm diameter). Impact spherules (*i.e.*, spheres or rounded bodies up to a few millimeters in size) are glassy spherules formed due to extraterrestrial impacts and represent a significant volume of the distal ejecta. By composition (Glass and Simonson, 2012; Glass, 2016), it is possible to define two types of impact spherules: (1) microtektites, which do not contain primary microlites, and (2) microkrystites (Glass and Burns, 1988), which have partly crystallized and contain microlites. According to their original definition, microtektites are melted in origin (Koeberl, 2002), although some authors (e.g., Elkins Tanton et al., 2002) considered it predominantly condensate droplets. In turn, it is assumed that microkrystites correspond to condensed droplets (Johnson and Melosh, 2012; Belza et al., 2017; Goderis et al., 2021), although depending on the composition of the melt and temperature history, microtektites can form from plume condensate droplets and microkrystites can be formed from melt ejecta droplets (Glass and Simonson, 2011). Most of the melted ejecta spherules are microtektites, and most of the spherules formed from condensate droplets are microkrystites.

Impact spherule beds form rapidly and can be distributed regionally or globally (e.g., the Cretaceous/Paleogene boundary - KPB); therefore, they represent excellent time-stratigraphic markers (Montanari and Koeberl, 2000; Simonson and Glass, 2004; Glass and Simonson, 2012; Vajda and Bercovici, 2014). The Chicxulub impact is an ideal case study since it is the only recognized impact event on Earth that preserved a globally traceable ejecta layer (Smit, 1999; Claeys et al., 2002; Schulte et al., 2010; Artemieva and Morgan, 2020; Goderis et al., 2021; Gulick, 2025), and it is the most likely cause of the KPB mass extinction (Arz et al., 2004; Arenillas et al., 2006; Molina et al., 2009; Schulte et al., 2010; Morgan et al., 2022; Chiarenza

and Brusatte, 2023). The Chicxulub impact expelled millions of tons of molten and vaporized materials in an impact plume and ejecta curtain, constituting, once settled, the global KPB deposits (Artemieva et al., 2017; Gulick et al., 2019; Morgan et al., 2022).

The global record of the KPB has been extensively studied since the discovery of the Chicxulub crater (Hildebrand et al., 1991). Overall, the stratigraphy and thickness of the KPB deposits vary with distance from the crater (Schulte et al., 2010), although local conditions and accommodation may affect thickness (Gulick, 2025). In proximal sites (< 1,000 km from Chicxulub's crater), the stratigraphy of the KPB deposits is complex, and the thickness varies depending on the amounts of remobilized sediments and subsequent re-deposition by several mechanisms such as impact-triggered tsunamis, submarine landslides, sediment fluidization and liquefaction, slumping or gravity flows (e.g., Bralower et al., 1998; Smit, 1999; Arz et al., 2001; Soria et al., 2001; Schulte et al., 2012; Denne et al., 2013; Sanford et al., 2016; Gulick, 2025). In the Gulf of Mexico and the Caribbean, the KPB deposits are generally fining-upward sedimentary successions with a metric or decametric thickness, although they can exceed hundreds of meters (Sanford et al., 2016; Christeson et al., 2021; Arz et al., 2022). For intermediate sites (1,000 - 5,000 km), the thickness of the KPB deposits ranges from centimeters to decimeters, showing a distinct dual-layer stratigraphy (Smit, 1999; DePalma et al., 2019; Gulick, 2025) in which the lower part is similar to spherule beds in proximal sites, while the upper part is comparable to the global distal ejecta layer (Artemieva and Morgan, 2009). Distal sites (> 5,000 km) record a thin (2 - 4 mm) ejecta layer known as the "fireball layer" (Bohor, 1990; Hildebrand and Boynton, 1990). The fireball layer is typically 2 to 4 mm thick and is characterized by abundant impact spherules presumably formed from vaporized target rock and meteorite materials, shocked minerals, and sediments enriched in platinum-group elements

(Johnson and Melosh, 2012). Importantly, this layer establishes a crucial temporal horizon that precisely links the Chicxulub impact to the KPB (Artemieva and Morgan, 2009; Belza et al., 2017; Claeys et al., 2002; Goderis et al., 2021). Nevertheless, the processes and mechanisms forming and transporting the ejecta to distal positions remain underconstrained. Some authors argue that the fireball layer represents shocked, metamorphosed mineral grains and condensed droplets from a vapor plume traversing the globe ballistically (Kring and Durda, 2002; Johnson and Melosh, 2012; Belza et al., 2017). This idea conflicts with three-dimensional numerical models and the stratigraphic record, as a purely ballistic distribution scenario is insufficient to explain a global boundary layer due to disparities in KPB bed thickness, ejection velocities, and the required volume of vaporized materials (Artemieva and Morgan, 2020).

Recognizing the importance of integrating physical evidence to understand the processes governing the formation and distribution of ejecta materials during the Chicxulub impact, we analyzed impact spherules from four high-fidelity KPB sites in North and South America and Western Europe. Our findings demonstrate that geological and sedimentological observations are key tools to provide direct, robust, and accurate information about ejecta features and the relation to distribution mechanisms. Here, we conduct a detailed sedimentological analysis of impact spherules from sites located at different distances from the crater to explore the connection between the spherule morphology, size, internal structure, and distribution within the KPB bed and the origin and potential transport mechanisms. This analysis sheds light on the processes that govern the global transport of Chicxulub-derived ejecta and will help improve recent ejecta distribution numerical models during massive asteroid impacts, allowing a better understanding of its influence on climatic and environmental changes at regional and global scales.

2. Geological setting

The samples studied were obtained from the bed representing the KPB in outcrops from Wahalak Creek, Mississippi, USA; Tanis, North Dakota, USA; Gorgonilla Island, Colombian Pacific; and Zumaia, Basque Country, northern Spain (Fig. 1). According to paleogeographic maps (Scotese, 2021), at the time of the KPB, the sites were located approximately 1,500 km north, 3,000 km north, 3,000 km south, and 7,000 km east of the Chicxulub crater, respectively.

The ~2-m-thick bed representing the KPB in Wahalak Creek (Fig. 2 A-C) corresponds to channelized deposits of sandstones and conglomerates with abundant macrofossils and impact spherules, interpreted as tsunami deposits, interbedded between the Danian Clayton Formation and the Maastrichtian Prairie Bluff Chalk Formation (Larina et al., 2016; Witts et al., 2018; Sosa-Montes de Oca et al., 2024). Due to poor preservation and limited exposure, small spherules from the upper part of these strata, which include fine sandstones and mudstones that potentially preserve the fireball layer, were not analyzed.

The ~ 1.3-m-thick bed representing the KPB in Tanis (Fig. 2 D-F) shows a normally graded sequence of coarse sandstone to siltstone/claystone that includes impact spherules and a mass death assemblage of diverse marine and terrestrial fossils. The ejecta-bearing sediments were emplaced by two massive impact-triggered surges during the first hours after the impact (DePalma et al., 2019; LeVeque et al., 2024). Evidence supporting the link to the Chicxulub impact is based on a geochemical match with unmelted Chicxulub glass found in other locations and a $^{40}Ar/^{39}Ar$ age of unmelted glass cores from altered spherules. This age is well aligned with Chicxulub melt-rock and spherules from different sites (DePalma et al., 2019). This bed overlies point bar deposits typical of the Hell Creek Formation and is overlain by a 1-2-cm-thick clay-altered layer (not studied here) corresponding to a smectitic tonstein, comparable to the "fireball

layer," enriched with spherules, shocked minerals, iridium, and other impact-derived materials (DePalma et al., 2019) representing the settling of fine debris long after the Chicxulub impact (Goderis et al., 2021).

The KPB bed at Gorgonilla Island (Fig. 2 G-I) corresponds to a normally graded ~2-cm-thick sequence of incredibly preserved glass spherules (Bermudez et al., 2016; Bermúdez et al., 2018), with an $^{40}Ar/^{39}Ar$ age of 66.051 ± 0.031 Ma (Renne et al., 2018). Gorgonilla Island impact spherules are virtually intact (up to 90% preserve the original glass and are not altered to clay minerals as other sites), representing the most pristine Chicxulub impact spherules known to date. The spherule-rich bed is interbedded between rhythmic intercalations of litharenites and tuffaceous marls, interpreted as deep-sea marine turbidites deposits (Bermudez et al., 2016; Bermúdez et al., 2018).

The KPB bed at Zumaia (Fig. 2 J-L) corresponds to a millimeter-thick red layer with impact spherules, overlain by a 9-cm-thick blackish claystone bed, interbedded between the Maastrichtian Zumaia-Algorri Formation reddish marls and the Danian Aitzgorri Formation red-pink marly limestones deposited in a middle bathyal setting (Gilabert et al., 2022).

3. Materials and methods

Considering that this contribution is focused on the study of morphological and morphometric aspects of Chicxulub impact-related droplets, here we use the generic term "impact spherules" (Glass, 2016) to describe the vitreous and altered droplets preserved in intermediate to distal deposits of the KPB. No distinctions are made regarding spherules' size, origin, or composition. KPB beds were gently disintegrated, and individual spherules were picked by hand under a Zeiss Stemi 508 Stereo Microscope in the Paleoclimatology lab at

Montclair State University. From the Wahalak Creek KPB bed, about 500 g of rock was disaggregated to obtain about 1,000 individual spherules, from which 900 were selected for morphological analysis. For the Tanis samples, approximately one cubic meter of sediment from the lower-middle graded surge pulse (unit 2) was disaggregated with water and a 0.5% hydrogen peroxide solution before passing through nested sieves. Spherules were hand-picked from the residuum, which consisted of coarse material and agglomerated fine sediment that remained after sieving, obtaining 200 individual spherules for morphological analysis. From the Gorgonilla Island KPB bed, about 200 g of rock was disaggregated to obtain over 5,000 individual spherules, from which 2,000 were randomly selected for morphological analysis. From the Zumaia KPB bed, about 100 g of rock was disaggregated to obtain about 300 individual spherules, from which 225 spherules were randomly selected for morphological analysis. Spherules were categorized using a morphological classification scheme based on previously published mathematical models (Fig. 3), numerical simulations, and experimental findings (Elkins-Tanton et al., 2003; Stauffer and Butler, 2010; Butler et al., 2011; Baldwin et al., 2015).

The photographic record of representative spherules was made using a 5MP Zeiss Axiocam 208 color camera. To provide further information on the morphological features of the impact spherules, additional photos of polished sections (Gorgonilla Island section) or individual spherules (Gorgonilla Island and Zumaia sections; Mississippi spherules are deemed too altered and unsuitable for SEM images) were taken under a Quanta FEG 650 scanning electron microscope (SEM) at the Department of Geosciences at the Swedish Museum of Natural History, Stockholm, Sweden (Gorgonilla spherules) and a Zeiss MERLIN FE-SEM in the Electron Microscopy Service of the Universidad de Zaragoza, Spain (Zumaia spherules).

For morphological classification, three categories were considered: 1) spheres, 2) rotational forms, and 3) agglutinated-irregular forms. Using models starting with spherical shapes, Fig. 3 illustrates the geometrical parameters and a new model that groups the shapes experimentally obtained by subjecting liquid droplets to rotation (Elkins-Tanton et al., 2003; Stauffer and Butler, 2010; Baldwin et al., 2015). The conditions necessary to obtain those shapes are explained below. Although our findings demonstrate the formation of all these rotational shapes within the spherules resulting from the Chicxulub impact, a detailed analysis of each morphology is beyond the scope of this research. Finally, the agglutinated-irregular forms include all morphologies resulting from the agglutination or irregular deformation of pre-existing spheres or rotational forms.

We consider three categories for size classification: 0.1 – 1 mm, 1 – 10 mm, and 10 – 100 mm size fractions. For the 0.1 – 1 mm size fraction, we count the total occurrence and proportion of the three shape categories every 0.1 mm increment. For the 1 – 10 mm size fraction, we estimate the percent of these shapes every 1 mm increment. For sizes larger than 10 mm, every 10 mm increment is considered.

4. The physics of the impact spherules

Impact spherules correspond to glassy droplets formed during asteroid impacts (Simonson and Glass, 2004; Johnson and Melosh, 2012). Impact spherules include diverse shapes that depend on the processes occurring during and after the flight before they undergo cooling and solidification (Simonson and Glass, 2004; Stauffer and Butler, 2010). The shape is related to the physics of liquid spinning droplets (bodies of revolution) following a transitional sequence that begins with a sphere and deforms through viscous fluid flow processes into other

shapes depending on surface tension and rotational velocity (Elkins-Tanton et al., 2003; Stauffer and Butler, 2010; Baldwin et al., 2015).

Physical parameters govern droplet dynamics and stability of spinning, as translating droplets during laboratory experiments demonstrated that moving droplets assume the form of bodies of rotation if rotational speed is only 1% or more of translational speed (Elkins-Tanton et al., 2003). Secondary processes (occurring during flight) include ablation, spalling, fragmentation, degassing, and bubble formation, while ground impact leads to plastic flattening, bending, and impact fragmentation. After landing, spalling and degassing may also occur (Stauffer and Butler, 2010). Additionally, it is important to note that collisions may occur during flight or at the time of deposition, deforming or causing the agglutination of one or more spherules if they have not yet solidified and also potentially increasing the incidence of unmelted inclusions if the fragments are appressed between the agglutinating spherules.

It has been experimentally demonstrated that increased dimensionless angular momentum allows a sphere to progressively evolve into oblate shapes, tri-axial ellipsoids, and finally, dumbbells, until unstable shapes are produced when the angular momentum is greater than 2.0, including theoretical triangular unstable equilibrium shapes for values between 2.0 and 2.8 (Elkins-Tanton et al., 2003; Stauffer and Butler, 2010; Baldwin et al., 2015).

In equilibrium (when pressure and centrifugal forces are precisely in balance everywhere inside the drop), the shape of a fluid drop is uniquely parameterized by the so-called Eötvös or Bond number. The Bond number is a non-dimensional number defined by the quotient of the gravitational forces and the forces due to surface tension (Elkins-Tanton et al., 2003; Stauffer and Butler, 2010). The Bond number is described in the following equation (Eq. 1):

$$B_0 = \rho\Omega^2 R^3/8\sigma. \quad (1)$$

Where ρ, Ω, and σ are the density, rotational frequency, and surface tension of the fluid drop. The variable R represents the radius of a sphere with the same volume as the drop.

It has been observed that there are no centrifugal forces at zero values of B_0 (a particular case when the rotational velocity is zero), and the surface tension creates perfectly spherical shapes for the spherules. B_0 values up to 0.09 produce approximately oblate ellipsoids. B_0 values between 0.09 and 0.31 allow both oblate ellipsoids and dumbbells. B_0 values greater than 0.31 allow for the development of unstable, in equilibrium, axisymmetric shapes, which become bi-concave when an angular momentum of 0.5 is exceeded, and a torus's shape is achieved when the B_0 value is at 0.57. Beyond 0.57, there are no equilibrium shapes, and the droplet will eventually pinch off into two or more drops (Stauffer and Butler, 2010; Butler et al., 2011). Alternatively, it has been proposed that based on the spin pattern and the spin rate, relatively rapid spin rates allow the evolution of spheres into rods and dumbbells, eventually separating into teardrops that, if maintaining sufficient fluidity, can again reach a spherical shape. At low spin rates, discs, bowls, and torus shapes evolve when central thinning develops (Beyer, 1962).

5. Results

The results of the shape and size distribution of the impact spherules (Table S1, Fig. 4, and Fig. 5) are based on 900, 200, 2,000, and 225 individual spherules from Wahalak Creek, Tanis, Gorgonilla Island, and Zumaia, respectively. Quantities vary according to absolute abundance and preservation. Only spherules from the high-energy deposits of the lower part of the KPB bed were studied in Wahalak Creek and Tanis. The thin deposits in the upper part of the KPB bed, although they include spherules, were not analyzed in this study due to poor preservation.

Our analysis is consequent with an increase in size in the direction of the crater (Fig. 5A) and reveals the occurrence of three different populations with a characteristic sedimentological signature (Fig. 5B-C). Spherules larger than 2 mm do not include spheres. Spherules of intermediate size (0.3 and 2 mm) involve variable proportions of spherical, rotational, and agglutinated/irregular forms. Finally, spherules smaller than 0.3 mm are composed of spheres only.

5.1.Wahalak Creek

At Wahalak Creek (Fig. 4G, 5A-B, and Table S1), impact spherules with sizes between 0.5 and 11 mm were identified. No spheres larger than 2 mm were observed. The proportion of spheres increases as the size decreases until it reaches 33.3% of the population in the 0.5-0.6 mm fraction. The proportion of rotational forms is variable but constitutes the most abundant morphology (> 70%) in the size fraction between 1 and 5 mm, where most of the impact spherules from this locality are concentrated (~88%). Rotational forms represent 100% of the population at sizes > 8 mm; however, they only include a few impact spherules. In fractions with sizes > 8 mm and < 1 mm, there are no agglutinated/irregular forms. The proportion of agglutinated/irregular forms is variable but never exceeds 50% of the population, which occurs in size fraction between 6-8 mm.

5.2. Tanis

At Tanis (Fig. 4E, 5A-B, and Table S1), impact spherules with sizes between 0.4 and 4 mm were observed. No spheres larger than 2 mm were observed. The proportion of spheres is variable but reaches 60% of the population in the 0.3-0.4 mm fraction. The proportion of

299 rotational forms is variable but constitutes the most abundant morphology (> 70%) in the size
300 fraction between 0.4 and 2 mm, where most of the spherules from this locality are concentrated
301 (~89%). No agglutinated/irregular forms were recognized for the spherules with sizes > 4 mm
302 and < 0.9 mm. The proportion of agglutinated/irregular forms increases with the size of the
303 spherules, reaching 50% of the population in the 3-4 mm fraction.
304
305 **5.3. Gorgonilla Island**
306 At Gorgonilla Island (Fig. 4F, 5A-B, Table S1), impact spherules with sizes between 0.2
307 and 5 mm were observed. No spheres larger than 2 mm were observed. The proportion of
308 spheres increases as the size decreases until it reaches 100% of the population in the finest
309 fraction (0.3-0.4 mm). Overall, the proportion of rotational forms increases with increasing size,
310 reaching 100% in the coarsest fraction (4-5 mm fraction) and constitutes the most abundant
311 morphology (> 50%) in the size fraction between 0.8 and 3 mm, where most of the spherules
312 from this locality are concentrated (~84%). As in the Tanis section, no agglutinated/irregular
313 forms were recognized in the size fraction > 4 mm and < 1 mm. The proportion of
314 agglutinated/irregular forms is variable but never exceeds 46% of the population, which occurs
315 only in the size fraction between 2-3 mm.
316
317 **5.4. Zumaia**
318 At Zumaia (Fig. 4D, 5A-B, Table S1), impact spherules with sizes between 0.1 and 3 mm
319 were observed, and unlike the previous localities, no agglutinated/irregular forms were identified
320 in any of the documented size fractions. Notably, no spheres larger than 1 mm were detected,
321 and the proportion increases as the size fraction decreases until it reaches 100% of the population

in the finest fractions (< 0.3 mm). Spherical shapes constitute the most abundant morphology (> 85%) in the fractions between 0.2 and 0.5 mm, where most of the spherules from this locality are concentrated (~90%). Overall, the proportion of rotational forms increases with increasing size, reaching 100% in the coarsest fractions (> 0.7 mm); however, these sizes only include a few impact spherules.

6. Discussion

Our analyses of the morphology, size, internal structure, and distribution of the impact spherules within the KPB bed from spatially variable sites can provide physical evidence which sheds light on the debate surrounding the transport mechanism of the Chicxulub impact ejecta and its global distribution. We identify three distinct populations within the KPB deposits by analyzing morphologically and morphometrically thousands of impact spherules deposited at intermediate and distal distances to the north, south, and east of the Chicxulub crater (Fig. 5A-B). These populations correspond to an idealized, normally graded tripartite sequence (Fig. 5C) when the deposits are complete and undisturbed, as occurs in a few sites such as Gorgonilla Island (Fig. 4F) or Demerara Rise (Schulte et al., 2009).

6.1. Sedimentologic signature of Chicxulub-associated impact spherules

The coarsest size fraction includes spherules larger than 2 mm and is composed exclusively of rotational and agglutinated/irregular forms (*i.e.*, no spheres). When the KPB deposits are complete and undisturbed, this population may constitute a basal deposit that we call the "aspergo deposit," a new term from the Latin *aspergo*, meaning splash. Spherules from the aspergo deposit were identified at all studied sites (Fig. 4 and Fig. 5), but only one was found at Zumaia (Table S1).

The intermediate fraction (0.3 to 2 mm in size) includes spheres, rotational, and agglutinated/irregular shapes and may comprise a transitional deposit that we call "pyrocloud deposit," a new term from the Greek *pyr*, meaning fire. Spherules from the pyrocloud deposit were identified at all sites studied (Table S1). This population has a transitional mixture of relatively large spherules, similar to those of the aspergo deposit, and relatively small spherules, similar to those of the fireball layer. Unlike the aspergo deposit, the large forms include spherules, while the smaller ones, distinct from the fireball layer, include rotational shapes (Fig. 4 and Fig. 5).

The finest fraction (size <0.3 mm) includes only spheres (i.e., no rotational or agglutinated/irregular forms) and is equivalent to the previously reported "fireball layer" from European and North American localities (Smit, 1999; Molina et al., 2006; Artemieva and Morgan, 2009; Belza et al., 2017). Spherules from the fireball layer were studied using samples from Gorgonilla Island and Zumaia KPB sections (Fig. 4, Fig. 5, and Table S1).

Combined, the aspergo deposit and the pyrocloud deposit constitute the totality of the spherules present in the high-energy geologically quasi-instantaneous KPB deposits (*i.e.,* deposited over minutes to hours) associated with the Chicxulub impact in positions relatively close to the Chicxulub crater in the Americas. Numerous authors describe these materials as the bottom of a "dual stratigraphy" for the KPB bed that at the top contains the globally distributed fireball layer (Smit, 1999; Artemieva and Morgan, 2009) deposited over much longer timescales (*e.g.,* months to years). We prefer the terms aspergo deposit and pyrocloud deposit to the classic "ejecta layer" proposed previously (Hildebrand and Boynton, 1990; Smit, 1999) because it defines more precisely the KPB deposit stratigraphy (e.g., there is also ejecta in the fireball layer).

All of the spherules in the aspergo deposit and most of the spherules in the coarser fraction of the pyrocloud deposit consist of rotational and agglutinated/irregular forms (*i.e.*, no spheres) with abundant vesicles, unmelted inclusions, and schlieren (Fig. 5A-B), suggesting an origin from molten materials. The morphologies observed indicate rotation during flight and frequent collisions. The shapes preserved in these populations reveal that the Bond number and the angular momentum were sufficient for the shapes to progress from spheres to oblong ellipsoids and more evolved morphologies (ovoids, rods, dumbbells, teardrops, bowls, and discs; see Fig. 3 and Fig. 4), implying that gravitational forces dominated over surface tension forces (Elkins-Tanton et al., 2003; Stauffer and Butler, 2010; Butler et al., 2011; Baldwin et al., 2015). Conversely, concave-convex contacts in numerous spherules at Gorgonilla Island (Fig. 4A-C) suggest several droplets arrived at high temperatures at the depositional site before sinking in the Pacific Ocean.

The totality of the spherules in the fireball layer and most of the spherules in the finer portion of the pyrocloud deposit consist exclusively of spheres of dense glass, lacking unmelted inclusions, vesicles, and schlieren (Fig. 4C), reflecting that collisions and rotation played no role in the formation and distribution of these spherules, and suggesting an origin from condensed materials. The absence of rotation indicates that the Bond number was close to zero (< 0.09), implying that surface tension forces dominated over gravitational forces, and the angular momentum was not large enough for the spheres to evolve to other morphologies (Elkins-Tanton et al., 2003; Stauffer and Butler, 2010; Butler et al., 2011; Baldwin et al., 2015).

6.2. Analysis of the weight of fractions/layers

In order to obtain an estimate of the weight distribution of each morphological category by size fraction, all impact spherules were considered spheres. Considering the average size of each size fraction, an average radius was estimated, which was used to calculate (Eq. 2) the volume (V) of an equivalent sphere and its respective weight according to a glass density value of 2.7g cm^{-3}. The values obtained are presented in Table S1. The Volume (V) is described in the following equation:

$$V = 4/3\ \pi\ r^3 \qquad (2)$$

Where π is a mathematical constant that is the ratio of a circle's circumference to its diameter, approximately equal to 3.14159, and the variable r represents a sphere's radius (in cm).

The impact spherules from the aspergo deposit represent 95.015%, 54.132%, 37.854%, and 37.796% of the weight of the KPB layer in Wahalak Creek, Tanis, Gorgonilla Island, and Zumaia, respectively. On the other hand, the impact spherules from the pyrocloud deposit represent 4.985%, 45.868%, 62.143%, and 60.193% of the weight of the KPB layer at Wahalak Creek, Tanis, Gorgonilla Island, and Zumaia, respectively. The weight of the spherules from the fireball layer in the sites where it was studied represented only 0.002% and 1.835% of the weight of the KPB layer in Gorgonilla Island and Zumaia, respectively (Table S1).

6.3. Implications for a global reconstruction of the ejecta dispersal

From a morphological point of view, the absence of spheres and the abundance of rotational and agglutinated/irregular forms present in the aspergo deposit are related to rotation and frequent collisions between two or more spherules liquid enough to fuse or deform, suggesting ballistic distribution (Fig. 6).

Molten and condensed materials coexisting in the pyrocloud deposit suggests the expansion of a fast-moving, scorching, and turbulent cloud (the "pyrocloud"), transporting melted and vaporized materials from the impact site (Fig. 6). The pyrocloud could reach distal positions (> 5,000 km), agreeing with numerical models suggesting that this cloud could have traveled up to 3 km/s after traversing 5,000 km from the impact site (Artemieva and Morgan, 2020). Spherules transported ballistically and by the lateral expansion of the pyrocloud could reach the studied sites within a few minutes to a few hours after the impact and may be included in tsunami or surge deposits in proximal to intermediate locations (<5,000 km). The stratigraphic record suggests that the catastrophic deposits triggered by the Chicxulub impact and the arrival of molten spherules ejected from Chicxulub were coincident and took place during the first hours after the impact (DePalma et al., 2019; Artemieva and Morgan, 2020; Senel et al., 2023; LeVeque et al., 2024). The lack of spherules smaller than 0.3 mm at Wahalak Creek and Tanis may imply that the high-energy deposits preserved there were deposited before the arrival of the fireball layer spherules.

We interpret, as in previous works (Johnson and Melosh, 2012; Belza et al., 2017; Goderis et al., 2021), that the spherules included in the fireball layer correspond to condensed droplets from the Chicxulub impact-derived plume (Fig. 6) supporting the conclusions of numerical models (Artemieva and Morgan, 2020). We did not find evidence (signs of rotation or collisions between spherules) indicating that these materials could have reached distal areas following ballistic trajectories or at high temperatures. The vapors included in the plume, rich in shocked minerals and sediments enriched in platinum-group elements, may only have cooled sufficiently over a few hours to days to allow condensation of the spherules (Toon et al., 2016), and the settling of the distal ejecta should have taken years (Vellekoop et al., 2014; Goderis et

al., 2021) excluding the possibility of being included in the catastrophic deposits that accumulated shortly after the Chicxulub impact. Condensation as the primary formation mechanism for the fireball layer is also suggested by the exclusive occurrence of homogeneous glass spherules in this layer (Fig 4C).

7. Conclusions

In this work, more than three thousand impact spherules directly related to the Chicxulub impact have been investigated from a morphological and morphometric point of view. Impact spherules were collected at the intermediate sites of Wahalak Creek and Tanis in the USA, Gorgonilla Island in the Colombian Pacific, and the distal site of Zumaia, northern Spain. At the time of the impact, these sites were located approximately 1,500 km north, 3,000 km north, 3,000 km south, and 7,000 km east of the Chicxulub crater, respectively.

The thorough analyses of the spherules by size range, morphological features, and internal structure allowed us to define three distinct populations of impact spherules: 1) a coarser fraction (aspergo deposit) containing rotational and agglutinated/irregular forms (size > 2mm) with abundant vesicles, unmelted inclusions, and schlieren, implies an origin from molten materials, rotation during flight and frequent collisions, that suggest a distribution mechanism following ballistic trajectories: 2) an intermediate fraction (pyrocloud deposit) representing a mixture of spheres, rotational, and agglutinated/irregular forms (size 0.3 - 2 mm), which morphology and internal structure suggest the complex interaction of spherules of molten and condensed origin, distributed by the expansion of a high-temperature turbulent cloud, and 3) a globally distributed fireball layer composed entirely of spheres (size < 0.3 mm) condensed from the Chicxulub plume.

The importance of the fractions in thickness and volume/weight varies with distance from the crater. The spherules' size and the deposits' thickness decrease with the distance from the impact site. The aspergo deposit constitutes most of the total weight of the impact spherules in the proximal sites, while the pyrocloud deposit represents most of the materials in the distal sites. The weight of the fireball layer is not significant.

Our work offers the first evidence that ballistic trajectories and a "scorching dense cloud" (the pyrocloud) reached Western Europe, *i.e.,* > 7,000 km from the Chicxulub crater during the minutes and hours following the Chicxulub impact; however, future work is needed to fully assess the extent of distribution of each of the proposed mechanisms.

Although the detailed study of Chicxulub impact spherule features (using three-dimensional samples) provides physical evidence and a better understanding of the processes in motion during massive asteroid impacts, it will be necessary to acquire and analyze more data from sites at different positions from the crater, including proximal and ultra distal locations.

Further physical and numerical modeling and detailed geochemical analyses of the different spherule types in other KPB sites around the globe might help us resolve how impact spherules are formed and transported. Understanding these processes will have implications for asteroid impacts on the Earth and other terrestrial planets with atmospheres.

Acknowledgments

We thank Parques Nacionales de Colombia for allowing access to Gorgona Island National Park and Paleoexplorer SAS for financial support. Gavin Kenny and Vivi Vajda are thanked for their assistance with SEM analyses. Reviews and comments by Joanna Morgan and Billy Glass provided helpful suggestions for improving early versions of this manuscript. We

thank Reinaldo Rojas, Sean Gulick, and James Witts for their helpful comments and suggestions, which greatly improved the quality of this manuscript. HB acknowledges the support provided by the Geological Society of America 2022 Graduate Student Research Grant and the International Association of Sedimentologists 2023 Postgraduate Grant Scheme. HB, MDP, and YC acknowledge the support provided by NSF grant EAR-2002370. This research is part of the grants PID2022-136233NB-I00 funded by MCIN/AEI/10.13039/501100011033 and by ERDF A way of making Europe, and DGA group E33_23R funded by the Aragonese Government and by ERDF A way of making Europe. VG acknowledges support from Ministerio de Universidades (MIU) and the European Union (Margarita Salas post-doctoral grant) funded by the European Union-NextGeneration EU. We acknowledge the use of the Servicio General de Apoyo a la Investigación-SAI, Universidad de Zaragoza, Spain, for providing scanning electron micrographs.

CRediT authorship contribution statement

Hermann D. Bermúdez: Conceptualization, Funding acquisition, Investigation, Methodology, Visualization, Writing – original draft, Writing – review and editing. **Liliana Bolívar**: Conceptualization, Funding acquisition, Investigation, Methodology, Writing – review and editing. **José A. Arz**: Investigation, Writing - review & editing. **Ignacio Arenillas**: Investigation, Writing - review & editing. **Vicente Gilabert**: Investigation, Writing - review & editing, **Robert DePalma**: Investigation, Writing - review & editing, **George Phillips**; Investigation, Writing -review & editing, **Maurizia De Palma**: Methodology. **Daniela Bermúdez**: Methodology, Investigation. **Clemencia Gómez**: Supervision. **Ying Cui**: Supervision, Writing - review & editing.

Declaration of competing interest

The authors declare that they have no known competing financial interests or personal relationships that could have appeared to influence the work reported in this paper.

507 **Figure captions**

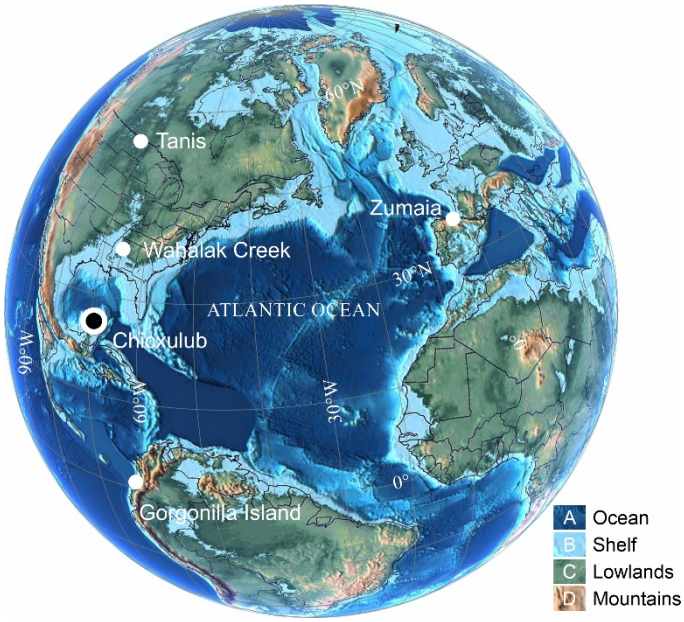

508

509 Fig. 1. Paleogeographic map for the KPB (Scotese, 2021) showing the locations of the studied

510 sites.

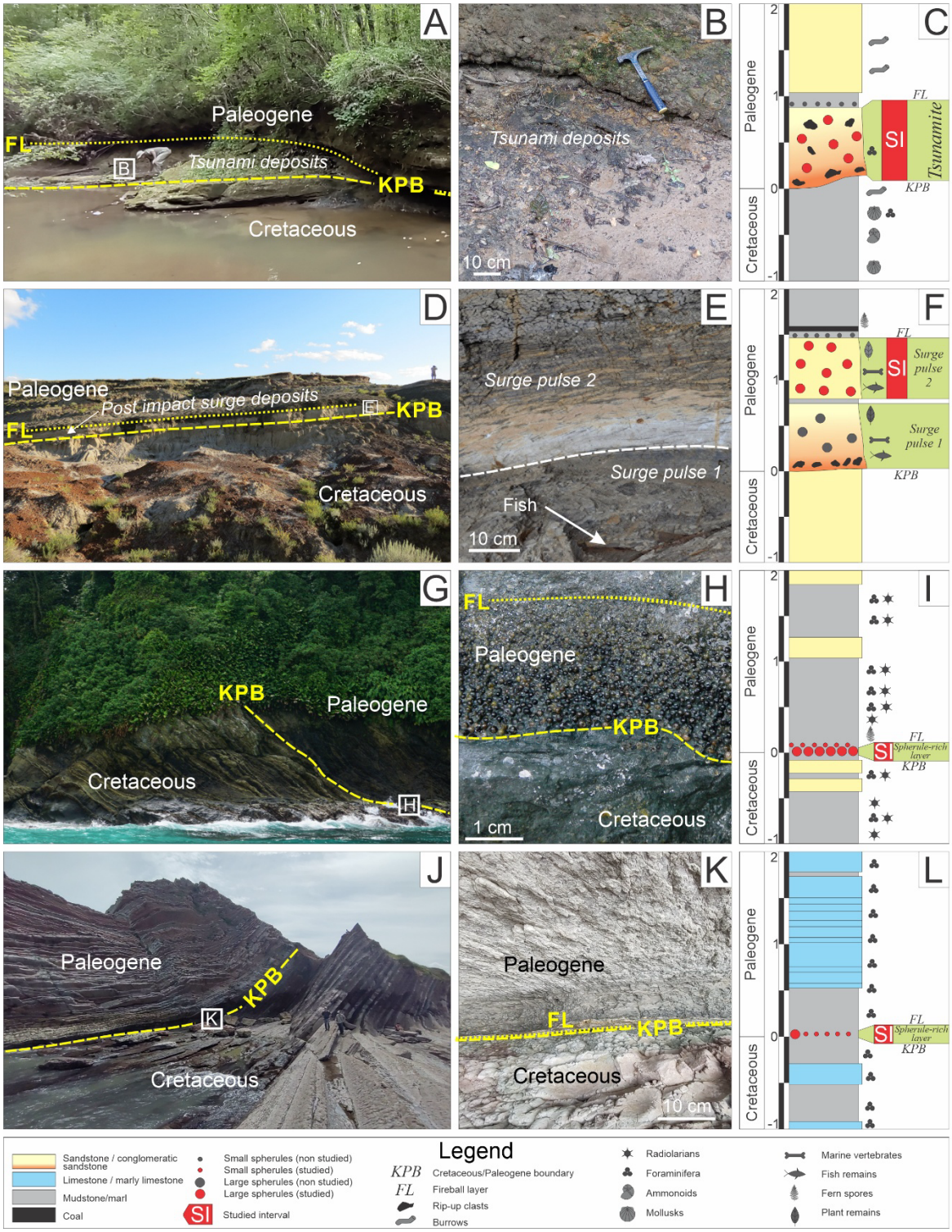

511

512 Fig. 2. Representative field photos (outcrop/detail) and stratigraphic column of the KPB sections
513 in Wahalak Creek (A-C), Tanis (D-F), Gorgonilla Island (G-I), and Zumaia (J-L). For the
514 stratigraphic section the scale is in meters.

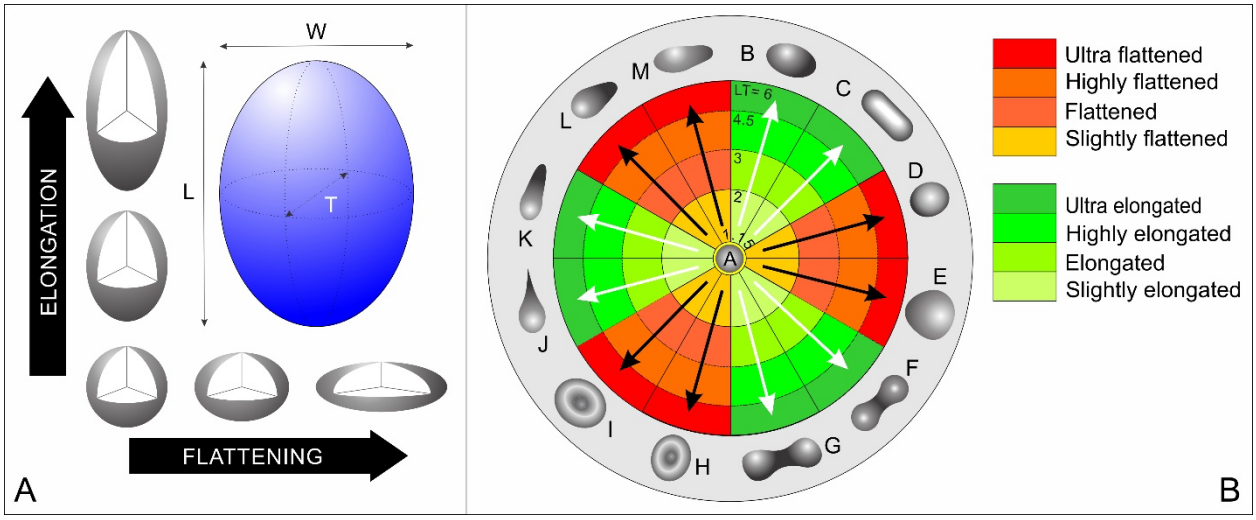

Fig. 3. A) Geometric parameters used to define ellipsoids: L= major axis, W= intermediate axis, T= thickness. The L/W ratio defines elongation. The W/T ratio defines flattening. B) New classification scheme for splash-form impact spherules. A= Spheres; B= Ovoids; C= Rods; D= Ovoid disks; E= Spherical disks; F= Dumbbells; G= Flattened dumbbells; H= Oval bowls; I= Circular bowls; J= Teardrops; K= Elongated teardrops; L= Ovoid teardrops; M= Flattened teardrops. The numbers represent values of the L/W ratio for elongation (green sectors and white arrows) and the W/T ratio for flattening (orange sectors and black arrows).

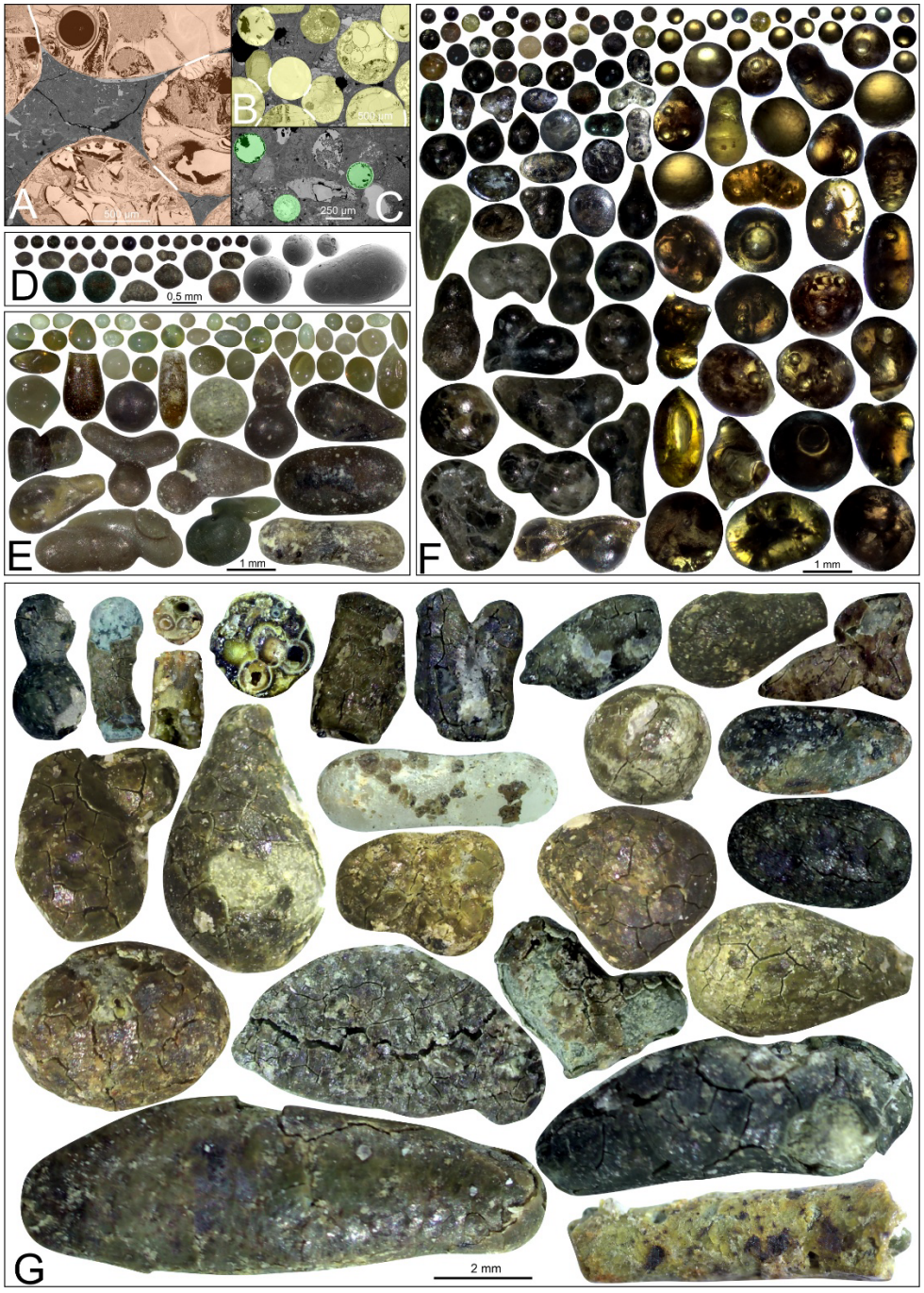

524

525 Fig. 4. Selected Chicxulub impact spherules. A-C) Backscattered electron images of typical
526 spherules from Gorgonilla Island showing concave-convex contacts (white lines). A) Bottom of
527 the KPB bed. B) Middle part of the KPB bed. C) Top of the KPB bed. D) Zumaia (including 5
528 Backscattered electron images on the right). E) Tanis. F) Gorgonilla Island (left: reflected light;
529 right: transmitted light). G) Wahalak Creek.

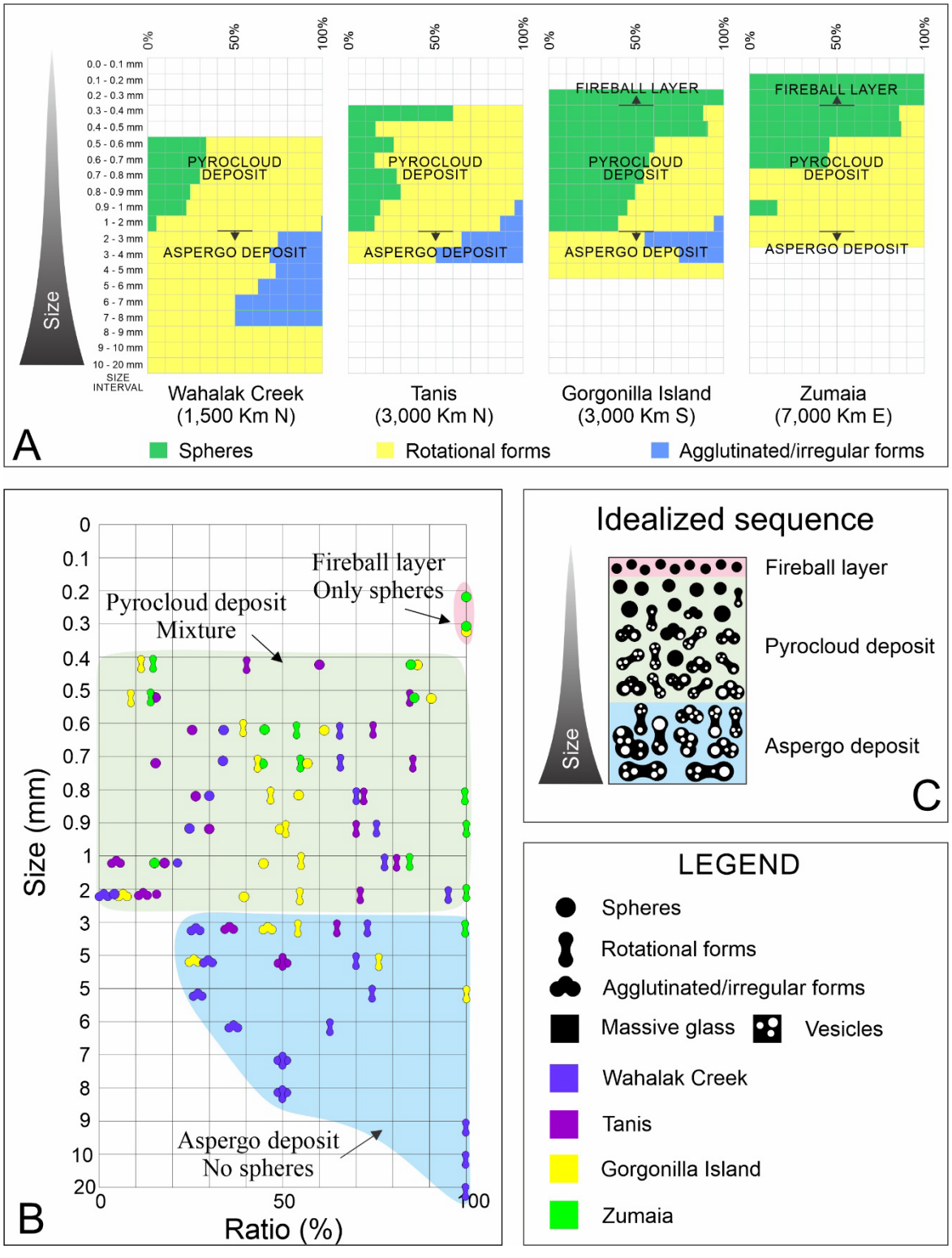

Fig. 5. Percent distribution of impact spherules by morphology and size. A) Results by site. B) Combined results. C) Idealized KPB bed sequence.

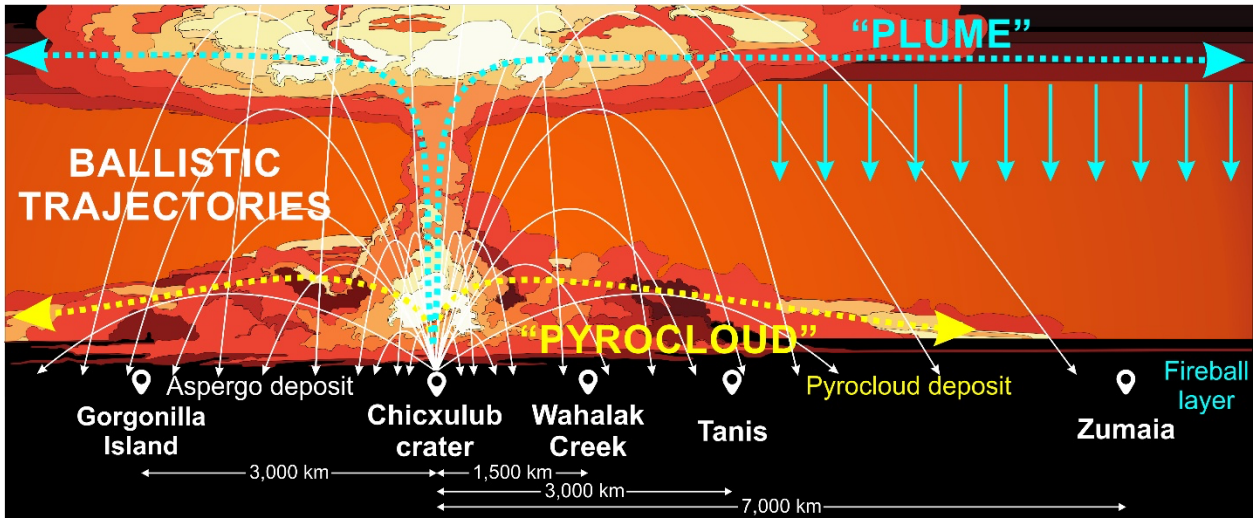

533

534 Fig. 6. Conceptual model of distribution mechanisms of molten and vaporized materials expelled

535 after the Chicxulub impact (not to scale).

536

537 **Supplemental Material**. Supplementary Table S1 (in a separate supplementary data file named

538 Table S1_Bermudez_et_al.xlsx.).

References

Arenillas, I., Arz, J.A., Grajales-Nishimura, J.M., Murillo-Muñetón, G., Alvarez, W., Camargo-Zanoguera, A., Molina, E., and Rosales-Domínguez, C., 2006, Chicxulub impact event is Cretaceous/Paleogene boundary in age: New micropaleontological evidence: Earth and Planetary Science Letters, v. 249, p. 241–257, https://doi.org/10.1016/j.epsl.2006.07.020

Arz, J.A., Arenillas, I., Soria, A.R., Alegret, L., Grajales-Nishimura, J.M., Liesa, C.L., Meléndez, A., Molina, E., and Rosales, M.C., 2001, Micropaleontology and Sedimentology of the Cretaceous/Paleogene boundary at La Ceiba (Mexico): impact-generated sediment gravity flows. Journal of South American Earth Sciences, v. 14, no 5, p. 505-519, https://doi.org/10.1016/S0895-9811(01)00049-9

Arz, J.A., Alegret, L., and Arenillas, I., 2004, Foraminiferal biostratigraphy and paleoenvironmental reconstruction at Yaxcopoil-1 drill hole (Chicxulub crater, Yucatan Peninsula). Meteoritics & Planetary Science, v. 39, no 7, p. 1099-1111, https://doi.org/10.1111/j.1945-5100.2004.tb01131.x

Arz, J.A., Arenillas, I., Grajales-Nishimura, J.M., Liesa, C.L., Soria, A.R., Rojas, R., Calmus, T., and Gilabert, V., 2022, No evidence of multiple impact scenario across the Cretaceous/Paleogene boundary based on planktic foraminiferal biochronology, in Koeberl, C., Claeys, P., and Montanari, A., eds., From the Guajira Desert to the Apennines, and from Mediterranean Microplates to the Mexican Killer Asteroid: Honoring the Career of Walter Alvarez: Geological Society of America Special Paper, v. 557, p. 415-448, https://doi.org/10.1130/2022.2557(20)

Artemieva, N., and Morgan, J. V., 2009, Modeling the formation of the K–Pg boundary layer: Icarus, v. 201, no. 2, p. 768-780, https://doi.org/10.1016/j.icarus.2009.01.021

562 Artemieva, N., and Morgan, J. V., 2020, Global K-Pg layer deposited from a dust cloud:
563 Geophysical Research Letters, v. 47, no. 6, p. e2019GL086562,
564 https://doi.org/10.1029/2019GL086562
565 Artemieva, N., Morgan, J. V., and Expedition 364 Science Party., 2017, Quantifying the release
566 of climate-active gases by large meteorite impacts with a case study of Chicxulub:
567 Geophysical Research Letters, v. 44, no. 20, p. 10,180-110,188,
568 https://doi.org/10.1002/2017GL074879
569 Baldwin, K. A., Butler, S. L., and Hill, R. J., 2015, Artificial tektites: an experimental technique
570 for capturing the shapes of spinning drops: Scientific reports, v. 5, no. 1, p. 1-5,
571 https://doi.org/10.1038/srep07660
572 Belza, J., Goderis, S., Montanari, A., Vanhaecke, F., and Claeys, P., 2017, Petrography and
573 geochemistry of distal spherules from the K–Pg boundary in the Umbria–Marche region
574 (Italy) and their origin as fractional condensates and melts in the Chicxulub impact
575 plume: Geochimica et Cosmochimica Acta, v. 202, p. 231-263,
576 https://doi.org/10.1016/j.gca.2016.12.018
577 Bermudez, H. D., Arenillas, I., Arz, J. A., Vajda, V., Renne, P. R., Gilabert, V., and Rodríguez,
578 J. V., 2018, The Cretaceous/Paleogene boundary deposits on Gorgonilla Island: The
579 Geology of Colombia, v. 3, p. 1-34, https://doi.org/10.32685/pub.esp.37.2019.01
580 Bermúdez, H. D., García, J., Stinnesbeck, W., Keller, G., Rodríguez, J. V., Hanel, M., Hopp, J.,
581 Schwarz, W. H., Trieloff, M., and Bolívar, L., 2016, The Cretaceous–Palaeogene
582 boundary at Gorgonilla Island, Colombia, South America: Terra Nova, v. 28, no. 1, p. 83-
583 90, https://doi.org/10.1111/ter.12196
584 Beyer, H., 1962, Philippine Tektites, Vol. 1 Part 2: Manila: University of The Philippines.

585 Bohor, B. F., 1990, Shocked quartz and more: Impact signatures in Cretaceous/Tertiary
586 boundary clays: Geological Society of America Special Papers, v. 247, p. 335-342.
587 Bralower, T. J., Paull, C. K., and Mark Leckie, R., 1998, The Cretaceous-Tertiary boundary
588 cocktail: Chicxulub impact triggers margin collapse and extensive sediment gravity
589 flows: Geology, v. 26, no. 4, p. 331-334, https://doi.org/10.1130/0091-
590 7613(1998)026<0331:TCTBCC>2.3.CO;2
591 Butler, S., Stauffer, M., Sinha, G., Lilly, A., and Spiteri, R., 2011, The shape distribution of
592 splash-form tektites predicted by numerical simulations of rotating fluid drops: Journal of
593 fluid mechanics, v. 667, p. 358-368, https://doi.org/10.1017/S0022112010005641
594 Chiarenza, A. A., and Brusatte, S. L., 2023, Dinosaurs, Extinction Theories for, Reference
595 Module in Life Sciences, Elsevier.
596 Christeson, G. L., Morgan, J. V., and Gulick, S. P. S., 2021, Mapping the Chicxulub Impact
597 Stratigraphy and Peak Ring Using Drilling and Seismic Data: Journal of Geophysical
598 Research: Planets, v. 126, no. 8, p. e2021JE006938.
599 Claeys, P., Kiessling, W., Alvarez, W., Koeberl, C., and MacLeod, K., 2002, Distribution of
600 Chicxulub ejecta at the Cretaceous-Tertiary boundary: Special Papers-Geological Society
601 of America, p. 55-68.
602 Denne, R. A., Scott, E. D., Eickhoff, D. P., Kaiser, J. S., Hill, R. J., and Spaw, J. M., 2013,
603 Massive Cretaceous-Paleogene boundary deposit, deep-water Gulf of Mexico: New
604 evidence for widespread Chicxulub-induced slope failure: Geology, v. 41, no. 9, p. 983-
605 986.
606 DePalma, R. A., Smit, J., Burnham, D. A., Kuiper, K., Manning, P. L., Oleinik, A., Larson, P.,
607 Maurrasse, F. J., Vellekoop, J., Richards, M. A., Gurche, L., and Alvarez, W., 2019, A

seismically induced onshore surge deposit at the KPg boundary, North Dakota: Proceedings of the National Academy of Sciences, v. 116, no. 17, p. 8190-8199, https://doi.org/10.1073/pnas.1817407116

Elkins Tanton, L., Kelly, D., Bico, J., and Bush, J., 2002, Microtektites as vapor condensates, and a possible new strewn field at 5 Ma, in Proceedings Lunar and Planetary Science Conference XXXIII (2002), p. 1622.

Elkins-Tanton, L. T., Aussillous, P., Bico, J., Quere, D., and Bush, J. W., 2003, A laboratory model of splash-form tektites: Meteoritics & Planetary Science, v. 38, no. 9, p. 1331-1340, https://doi.org/10.1111/j.1945-5100.2003.tb00317.x

Glass, B. P., 2016, Glass: The geologic connection: International Journal of Applied Glass Science, v. 7, no. 4, p. 435-445.

Glass, B., and Burns, C. A., 1988, Microkrystites-A new term for impact-produced glassy spherules containing primary crystallites, in Proceedings IN: Lunar and Planetary Science Conference, 18th, Houston, TX, Mar. 16-20, 1987, Proceedings (A89-10851 01-91). Cambridge and New York/Houston, TX, Cambridge University Press/Lunar and Planetary Institute, p. 455-458.1988, Volume 18, p. 455-458.

Glass, B. P., and Simonson, B. M., 2011, Variation in Distal Impact Ejecta with Distance from the Source Crater: A Model: Meteoritics and Planetary Science Supplement, v. 74, p. 5035.

Glass, B. P., and Simonson, B. M., 2012, Distal impact ejecta layers: Spherules and more: Elements, v. 8, no. 1, p. 43-48, https://doi.org/10.2113/gselements.8.1.43

Glass, B. P., and Simonson, B. M., 2013, Distal impact ejecta layers: A record of large impacts in sedimentary deposits, Springer Science & Business Media.

631 Gilabert, V., Batenburg, S. J., Arenillas, I., and Arz, J. A., 2022, Contribution of orbital forcing
632 and Deccan volcanism to global climatic and biotic changes across the Cretaceous-
633 Paleogene boundary at Zumaia, Spain: Geology, v. 50, no. 1, p. 21-25,
634 https://doi.org/10.1130/G49214.1
635 Goderis, S., Sato, H., Ferrière, L., Schmitz, B., Burney, D., Kaskes, P., Vellekoop, J., Wittmann,
636 A., Schulz, T., Chernonozhkin, S. M., Claeys, P., de Graaff, S. J., Déhais, T., de Winter,
637 N. J., Elfman, M., Feignon, J. G., Ishikawa, A., Koeberl, K., Kristiansson, P., Neal, C. R.,
638 Owens, J. D., Schmieder, M., Sinnesael, M., Vanhaecke, F., Van Malderen, S. J. M.,
639 Bralower, T. J., Gulick, S.P., Kring, D. A., Lowery, C. M., Morgan, J. V, Smit, J.,
640 Whalen, M. T., and IODP-ICDP Expedition 364 Scientists., 2021, Globally distributed
641 iridium layer preserved within the Chicxulub impact structure: Science advances, v. 7,
642 no. 9, p. eabe3647, https://doi.org/10.1126/sciadv.abe3647
643 Gulick, S. P., Bralower, T. J., Ormö, J., Hall, B., Grice, K., Schaefer, B., Lyons, S., Freeman, K.
644 H., Morgan, J. V., and Artemieva, N., 2019, The first day of the Cenozoic: Proceedings
645 of the National Academy of Sciences, v. 116, no. 39, p. 19342-19351.Hildebrand, A. R.,
646 and Boynton, W. V., 1990, Proximal Cretaceous-Tertiary Boundary Impact Deposits in
647 the Caribbean: Science, v. 248, no. 4957, p. 843-847,
648 https://doi.org/10.1126/science.248.4957.84
649 Gulick, S. P. S., 2025, End of the Cretaceous: Geological Society, London, Special Publications,
650 v. 544, no. 1, p. SP544-2023-2176.
651 Hildebrand, A. R., and Boynton, W. V., 1990, Proximal Cretaceous-Tertiary Boundary Impact
652 Deposits in the Caribbean: Science, v. 248, no. 4957, p. 843-847.

653 Hildebrand, A. R., Penfield, G. T., Kring, D. A., Pilkington, M., Camargo Z, A., Jacobsen, S. B.,
654 and Boynton, W. V., 1991, Chicxulub crater: a possible Cretaceous/Tertiary boundary
655 impact crater on the Yucatan Peninsula, Mexico: Geology, v. 19, no. 9, p. 867-871.
656 Johnson, B. C., and Melosh, H. J., 2012, Formation of spherules in impact produced vapor
657 plumes: Icarus, v. 217, no. 1, p. 416-430, https://doi.org/10.1016/j.icarus.2011.11.020
658 Koeberl, C., 1986, Geochemistry of tektites and impact glasses: Annual Review of Earth and
659 Planetary Sciences, v. 14, no. 1, p. 323-350.
660 Koeberl, C., 2002, Mineralogical and geochemical aspects of impact craters: Mineralogical
661 Magazine, v. 66, no. 5, p. 745-768.
662 Kring, D. A., and Durda, D. D., 2002, Trajectories and distribution of material ejected from the
663 Chicxulub impact crater: Implications for postimpact wildfires: Journal of Geophysical
664 Research: Planets, v. 107, no. E8, p. 6-1-6-22, https://doi.org/10.1029/2001JE001532
665 Larina, E., Garb, M., Landman, N., Dastas, N., Thibault, N., Edwards, L., Phillips, G., Rovelli,
666 R., Myers, C., and Naujokaityte, J., 2016, Upper Maastrichtian ammonite biostratigraphy
667 of the Gulf Coastal Plain (Mississippi Embayment, southern USA): Cretaceous Research,
668 v. 60, p. 128-151.
669 LeVeque, R. J., DePalma, R. A., Garrison-Laney, C., Maurya, S., Smit, J., and Richards, M. A.,
670 2024, Possible Mechanisms for Tsunami-Like Surge Deposits Due To the Chicxulub
671 Impact at the K-Pg Boundary at the Tanis Site, North Dakota: Journal of Geophysical
672 Research: Solid Earth, v. 129, no. 5, p. e2023JB027643.
673 Melosh, H. J., 1989, Impact cratering: A geologic process: New York: Oxford University Press;
674 Oxford: Clarendon Press.

675 Molina, E., Alegret, L., Arenillas, I., Arz, J.A., Gallala, N., Hardenbol, J., von Salis, K.,
676 Steurbaut, E., Vandenberghe, N., and Zaghbib-Turki, D., 2006, The global boundary
677 stratotype section and point for the base of the Danian stage (Paleocene, Paleogene,
678 "Tertiary," Cenozoic) at El Kef, Tunisia - Original definition and revision. Episodes, v.
679 29, no. 4, p. 263-273, https://doi.org/10.18814/epiiugs/2006/v29i4/004
680 Molina, E., Alegret, L., Arenillas, I., Arz, J. A., Gallala, N., Grajales-Nishimura, J. M., Murillo-
681 Muñetón, G., and Zaghbib-Turki, D., 2009, The Global Boundary Stratotype Section and
682 Point for the base of the Danian Stage (Paleocene, Paleogene, "Tertiary", Cenozoic):
683 Auxiliary sections and correlation: Episodes, v. 32, p. 84–95,
684 https://doi.org/10.18814/epiiugs/2009/v32i2/002.
685 Montanari, A., and Koeberl, C., 2000, Impact stratigraphy: the Italian record, Springer Science &
686 Business Media.
687 Morgan, J. V., Bralower, T. J., Brugger, J., and Wünnemann, K., 2022, The Chicxulub impact
688 and its environmental consequences: Nature Reviews Earth & Environment, v. 3, no. 5,
689 p. 338-354, https://doi.org/10.1038/s43017-022-00283-y
690 Osinski, G. R., Grieve, R. A. F., Ferrière, L., Losiak, A., Pickersgill, A. E., Cavosie, A. J.,
691 Hibbard, S. M., Hill, P. J. A., Bermudez, J. J., Marion, C. L., Newman, J. D., and
692 Simpson, S. L., 2022, Impact Earth: A review of the terrestrial impact record: Earth-
693 Science Reviews, v. 232, p. 104112, https://doi.org/10.1016/j.earscirev.2022.104112
694 Pierazzo, E., and Artemieva, N., 2012, Local and global environmental effects of impacts on
695 Earth: Elements, v. 8, no. 1, p. 55-60.
696 Reihart, J. S., 1958, Impact effects and tektites: Geochimica et Cosmochimica Acta, v. 14, no. 4,
697 p. 287-290.

698 Renne, P. R., Arenillas, I., Arz, J. A., Vajda, V., Gilabert, V., and Bermúdez, H. D., 2018, Multi-
699 proxy record of the Chicxulub impact at the Cretaceous-Paleogene boundary from
700 Gorgonilla Island, Colombia: Geology, v. 46, no. 6, p. 547-550,
701 https://doi.org/10.1130/G40224.1
702 Sanford, J. C., Snedden, J. W., and Gulick, S. P. S., 2016, The Cretaceous-Paleogene boundary
703 deposit in the Gulf of Mexico: Large-scale oceanic basin response to the Chicxulub
704 impact: Journal of Geophysical Research: Solid Earth, v. 121, no. 3, p. 1240-1261.
705 Schmieder, M., and Kring, D. A., 2020, Earth's impact events through geologic time: a list of
706 recommended ages for terrestrial impact structures and deposits: Astrobiology, v. 20, no.
707 1, p. 91-141.
708 Schulte, P., Deutsch, A., Salge, T., Berndt, J., Kontny, A., MacLeod, K., Neuser, R., and
709 Krumm, S., 2009, A dual-layer Chicxulub ejecta sequence with shocked carbonates from
710 the Cretaceous–Paleogene (K–Pg) boundary, Demerara Rise, western Atlantic:
711 Geochimica et Cosmochimica Acta, v. 73, no. 4, p. 1180-1204.
712 Schulte, P., Schulte, P., Alegret, L., Arenillas, I., Arz, J. A., Barton, P. J., Bown, P. R., Bralower,
713 T. J., Christeson, G. L., Claeys, P., Cockell, C. S., Collins, G. S., Deutsch, A., Goldin, T.
714 J., Goto, K., Grajales-Nishimura, J. M., Grieve, R. A. F., Gulick, S. P. S., Johnson, K. R.,
715 Kiessling, W., Koeberl, C., Kring, D. A., MacLeod, K. G., Matsui, T., Melosh, J.,
716 Montanari, A., Morgan, J. V., Neal, C.R., Nichols, D.J., Norris, R.D., Pierazzo, E.,
717 Ravizza, G., Rebolledo-Vieyra, M., Reimold, W.U., Robin, E., Salge, T., Speijer, R.P.,
718 Sweet, A.R., Urrutia-Fucugauchi, J., Vajda, V., Whalen, M.T., Willumsen, P.S., 2010,
719 The Chicxulub asteroid impact and mass extinction at the Cretaceous-Paleogene

boundary: Science, v. 327, no. 5970, p. 1214-1218, https://doi.org/10.1126/science.1177265

Scotese, C. R., 2021, An Atlas of Phanerozoic Paleogeographic Maps: The Seas Come In and the Seas Go Out: Annual Review of Earth and Planetary Sciences, v. 49, no. 1, p. 679-728, https://doi.org/10.1146/annurev-earth-081320-064052

Senel, C. B., Kaskes, P., Temel, O., Vellekoop, J., Goderis, S., DePalma, R., Prins, M. A., Claeys, P., and Karatekin, Ö., 2023, Chicxulub impact winter sustained by fine silicate dust: Nature Geoscience, 16, 1033–1040, https://doi.org/10.1038/s41561-023-01290-4

Simonson, B. M., and Glass, B. P., 2004, Spherule layers—Records of ancient impacts: Annu. Rev. Earth Planet. Sci., v. 32, p. 329-361, https://doi.org/10.1146/annurev.earth.32.101802.120458

Smit, J., 1999, The global stratigraphy of the Cretaceous-Tertiary boundary impact ejecta: Annual Review of Earth and Planetary Sciences, v. 27, no. 1, p. 75-113, https://doi.org/10.1146/annurev.earth.27.1.75

Soria, A.R., Liesa, C.L., Mata, M.P., Arz, J.A., Alegret, L., Arenillas, I., and Melendez, A., 2001, Slumping and a sandbar deposit at the Cretaceous-Tertiary boundary in the El Tecolote section (northeastern Mexico): An impact-induced sediment gravity flow: Geology, v. 29, p. 231-234, https://doi.org/10.1130/00917613(2001)029<0231:SAASDA>2.0.CO;2.

Sosa-Montes de Oca, C., Witts, J. D., Lowery, C. M., Kearns, L. E., Garb, M. P., Naujokaityte, J., Myers, C. E., Landman, N. H., and Pancost, R. D., 2024, Intense Changes in the Main Source of Organic Carbon to the Gulf Coastal Plain Following the Cretaceous-Paleogene Boundary: Paleoceanography and Paleoclimatology, v. 39, no. 8, p. e2024PA004887.

743 Stauffer, M. R., and Butler, S. L., 2010, The shapes of splash-form tektites: their geometrical
744 analysis, classification and mechanics of formation: Earth, Moon, and Planets, v. 107, no.
745 2-4, p. 169-196, https://doi.org/10.1007/s11038-010-9359-y
746 Suess, F. E., 1900, Die Herkunft der Moldavite und verwandter Gläser, Geologischen
747 Reichsanstalt.
748 Toon, O. B., Bardeen, C., and Garcia, R., 2016, Designing global climate and atmospheric
749 chemistry simulations for 1 and 10 km diameter asteroid impacts using the properties of
750 ejecta from the K-Pg impact: Atmospheric Chemistry and Physics, v. 16, no. 20, p.
751 13185-13212, https://doi.org/10.5194/acp-16-13185-2016
752 Vajda, V., and Bercovici, A., 2014, The global vegetation pattern across the Cretaceous–
753 Paleogene mass extinction interval: A template for other extinction events: Global and
754 Planetary Change, v. 122, p. 29-49.
755 Vellekoop, J., Sluijs, A., Smit, J., Schouten, S., Weijers, J. W., Damsté, J. S. S., and Brinkhuis,
756 H., 2014, Rapid short-term cooling following the Chicxulub impact at the Cretaceous–
757 Paleogene boundary: Proceedings of the National Academy of Sciences, v. 111, no. 21, p.
758 7537-7541, https://doi.org/10.1073/pnas.1319253111
759 Witts, J. D., Landman, N. H., Garb, M. P., Boas, C., Larina, E., Rovelli, R., Edwards, L. E.,
760 Sherrell, R. M., and Cochran, J. K., 2018, A fossiliferous spherule-rich bed at the
761 Cretaceous–Paleogene (K–Pg) boundary in Mississippi, USA: implications for the K–Pg
762 mass extinction event in the Mississippi Embayment and Eastern Gulf Coastal Plain:
763 Cretaceous Research, v. 91, p. 147-167, https://doi.org/10.1016/j.cretres.2018.06.002